Fluorine Abundances in the Galactic Nuclear Star Cluster

Rafael Guerço, Solange Ramírez, Katia Cunha, Verne V. Smith, Nikos Prantzos, Kris Sellgren, Simone Daflon

CrossMark

Fluorine Abundances in the Galactic Nuclear Star Cluster

Rafael Guerço[1] , Solange Ramírez[2], Katia Cunha[1,3] , Verne V. Smith[4] , Nikos Prantzos[5] , Kris Sellgren[6] , and
Simone Daflon[1]
[1] Observatório Nacional, São Cristóvão, Rio de Janeiro, Brazil; guercorafael@gmail.com
[2] Carnegie Observatories, Pasadena, CA 91107, USA
[3] University of Arizona, Tucson, AZ 85719, USA
[4] NOIRLAB, Tucson, AZ 85719 USA
[5] Institut d'Astrophysique de Paris, France
[6] The Ohio State University, Columbus, OH 43210, USA

Abstract

Abundances of fluorine (^{19}F), as well as isotopic ratios of ^{16}O/^{17}O, are derived in a sample of luminous young ($\sim 10^7$–10^8 yr) red giants in the Galactic center (with galactocentric distances ranging from 0.6–30 pc), using high-resolution infrared spectra and vibration-rotation lines of H^{19}F near $\lambda 2.3 \ \mu$m. Five of the six red giants are members of the Nuclear star cluster that orbits the central supermassive black hole. Previous investigations of the chemical evolution of ^{19}F in Galactic thin and thick-disk stars have revealed that the nucleosynthetic origins of ^{19}F may be rather complex, resulting from two, or more, astrophysical sites; fluorine abundances behave as a primary element with respect to Fe abundances for thick-disk stars and as a secondary element in thin-disk stars. The Galactic center red giants analyzed fall within the thin-disk relation of F with Fe, having near-solar, to slightly larger, abundances of Fe ($\langle$[Fe/H]$\rangle = +0.08 \pm 0.04$), with a slight enhancement of the F/Fe abundance ratio ($\langle$[F/Fe]$\rangle = +0.28 \pm 0.17$). In terms of their F and Fe abundances, the Galactic center stars follow the thin-disk population, which requires an efficient source of ^{19}F that could be the winds from core-He burning Wolf–Rayet stars, or thermally pulsing AGB stars, or a combination of both. The observed increase of [F/Fe] with increasing [Fe/H] found in thin-disk and Galactic center stars is not predicted by any published chemical evolution models that are discussed, thus a quantitative understanding of yields from the various possible sources of ^{19}F remains unknown.

Unified Astronomy Thesaurus concepts: Spectroscopy (1558); Stellar abundances (1577); Giant stars (655); Galactic center (565); Infrared telescopes (794); Chemical abundances (224)

1. Introduction

Mapping detailed chemical abundance patterns in the diverse stellar populations that compose the Milky Way can reveal details about the formation and evolution of both specific stellar populations, as well as that of the Milky Way itself, along with deeper insights into stellar nucleosynthesis and evolution. Among the elements heavier than hydrogen and helium, the quartet of carbon ($Z = 6$), nitrogen ($Z = 7$), oxygen ($Z = 8$), and neon ($Z = 10$) are, by far, the most abundant in number (as well as mass) and are crucial elements in understanding chemical evolution across the universe. Nestled within these four abundance peaks in the periodic table lies fluorine ($Z = 9$), whose abundance is ~four orders-of-magnitude smaller than its periodic table neighbors; from carbon and beyond, the solar system abundance of ^{19}F (the sole stable fluorine isotope) remains the smallest until scandium ($Z = 21$). Despite its relatively low abundance, fluorine isotopes play a key role in important H-burning (proton capture) reactions involving the various CNO cycles and Ne-Na cycles, which set the relative abundances of the isotopes of C, N, O, Ne, and Na. Compared to its abundant neighbors, the astrophysical origins of ^{19}F remain relatively unconstrained due to a combination of observational challenges, along with a variety of potential sites for its nucleosynthesis.

The earliest abundance determinations of fluorine were in red giant stars (e.g., Jorissen et al. 1992; Cunha et al. 2003; Smith et al. 2005; Cunha et al. 2008; Yong et al. 2008) and highlighted the challenges in observing fluorine abundance indicators in stars, due to the combination of its low abundance and atomic structure; these early studies used vibration-rotation transitions of H^{19}F in the near-infrared (NIR) K band, near $\lambda 2.3 \ \mu$m, which required high-resolution NIR spectrographs. The early studies probed samples of bright field red giant branch (RGB) and cool asymptotic giant branch (AGB) stars, along with small numbers of luminous red giant members of globular clusters, the Galactic bulge, or the LMC. As several studies derived moderate enhancements of fluorine abundances in TP-AGB stars (e.g., Jorissen et al. 1992; Uttenthaler et al. 2008; Abia et al. 2009, 2010, 2015), these studies suggested that AGB stars were one possible source of ^{19}F, but not necessarily the dominant source in the Galaxy (e.g., Spitoni et al. 2018; Grisoni et al. 2020).

In addition to observations of HF in cool red giant stars, the ground-state neutral fluorine line, F I at $\lambda 954$ Å, was detected in the interstellar medium (ISM) along three lines of sight by Federman et al. (2005) using the FUSE satellite. Federman et al. (2005) determined current ISM abundance ratios of F/Cl and F/O that were solar, within the measurement uncertainties. High-excitation ($\chi = 12.7$–13.0 eV) F I optical lines were also detected in several extreme helium (EHe) stars by Pandey (2006), and RCrB stars by Pandey et al. (2008), who found F to be very overabundant, by ~1000–8000 times, in these stars. As EHe and RCrB stars are likely in the post-AGB phase of evolution, these results implicated the post-AGB phase of stellar evolution as a potential source of

Table 1
Galactic Center Stars

Star	2MASS ID	Spectrograph	Observation (NIRSpec)	Observation (Phoenix)	J	H	K_s
BSD 72	⋯	NIRSpec/Phoenix	2001/8/16	2002/5/11	12.79	10.32	9.05[a]
BSD 124	17454240-2859510	NIRSpec/Phoenix	2001/8/16	2002/5/11	14.92	10.98	8.97
IRS 11	17453938-2900148	Phoenix	⋯	2002/5/11	15.12	10.62	8.35
IRS 19	⋯	NIRSpec	2001/8/15	⋯	14.81	10.83	8.22[a]
IRS 22	17453982-2900539	NIRSpec	2000/5/23	⋯	14.20	9.65	7.39
VR 5-7[b]	17461658-2849498	NIRSpec	2001/6/13	⋯	13.06	9.31	7.47

Notes.
[a] Soubiran et al. (2016).
[b] Member of the Quintuplet cluster.

fluorine. Werner et al. (2006) and Werner & Herwig (2006) pushed fluorine detections to the extremely hot H-deficient post-AGB stars by analyzing the F VI line at $\lambda1139.5$ Å using FUSE, also finding large F overabundances. More recently, Bhowmick et al. (2020) determined fluorine abundances in a number of hot EHe stars using optical F II lines and again found very large overabundances which, when compared to the abundances of C, O, and Ne, suggest that ^{19}F production in these stars results from the merger of a CO white dwarf with a He white dwarf (creating the hot EHe star), as modeled by Menon et al. (2013, 2019) and Lauer et al. (2019).

Although the observational studies noted above that derive fluorine overabundances in TP-AGB stars may point to them as net sources of ^{19}F in the Galaxy (e.g., Jorissen et al. 1992; Uttenthaler et al. 2008; Abia et al. 2015, 2019), as well as certain types of merging white dwarf binary systems (e.g., Clayton et al. 2007; Menon et al. 2013; Lauer et al. 2019; Menon et al. 2019; Bhowmick et al. 2020), there remain additional viable sources of ^{19}F that likely contribute to significant fluorine production in the Galaxy, yet remain difficult to quantify from observations. Such sources include the scattering of neutrinos off of ^{20}Ne during SN II core collapse (neutrino nucleosynthesis, or the ν-process), as discussed by Woosley & Haxton (1988) and Woosley et al. (1990). Massive stars undergoing large mass-loss rates during core-He burning (Wolf–Rayet (W-R) stars) were suggested by Meynet & Arnould (2000) as ^{19}F sources, although the efficacy of this source was studied in more detail by Palacios et al. (2005). Modeling by Prantzos et al. (2018) found that rapidly rotating high-mass stars can also synthesize ^{19}F and may be a significant source in the Galaxy. Several studies have included all of these potential sources of ^{19}F and incorporated them into models of Galactic chemical evolution that predict trends of, typically, [F/Fe] versus [Fe/H], or [F/O] versus [O/H], e.g., Timmes et al. (1995), (Kobayashi et al. 2011a, 2011b), Prantzos et al. (2018), Spitoni et al. (2018), and Grisoni et al. (2020).

Several recent observational studies have focused on determining the behavior of the fluorine abundance as a function of either the Fe or O abundances in order to constrain the chemical evolution of ^{19}F in the Galaxy, e.g., (Jönsson et al. 2014a, 2014b), Pilachowski & Pace (2015), Jönsson et al. (2017), Guerço et al. (2019), or Ryde et al. (2020). All of these works observed red giant stars and used vibration-rotation lines of HF in the $\lambda2.2$–2.4 μm, while Jönsson et al. (2014b) also included pure rotational lines of HF near $\lambda12$ μm. A takeaway summary of the recent observational results would note that the behavior of fluorine abundances as a function of either the Fe or O abundances is not fixed and varies over metallicity and possibly stellar population, indicating more than one

astrophysical source for ^{19}F (e.g., Ryde et al. 2020), as suggested by both the nuclear astrophysics and modeling.

Franco et al. (2021) recently added a new approach to mapping F abundances by using the Atacama Large Millimeter/submillimeter Array to detect ISM HF in absorption in a lensed star-forming galaxy at a redshift of $z = 4.42$ to obtain a measurement of the F/H abundance in the young universe. The detected line is the $J = 1 \rightarrow 0$ transition of HF with a rest wavelength of $\lambda243.2433$ μm. Values of [F/H] were estimated from ratios of N(HF)/N(H$_2$), with the authors noting that the derived abundance of F represents a lower limit. The values of N(HF) from Franco et al. (2021) translate to a lower limit of [F/H] ~ -1.4 in the ISM of this star-forming galaxy at $z = 4.42$, or a time when the universe was roughly 1 Gyr old. Franco et al. (2021) use a chemical evolution model that includes the ν-process, AGB stars, and rapidly rotating massive W-R stars, with the conclusion that in this young star-forming galaxy, rapidly rotating massive W-R stars are the major source of the observed ^{19}F abundance. In the adopted chemical evolution model from Franco et al. (2021), AGB stars and the ν-process are important sources of fluorine, but their contributions occur at later times (corresponding to redshifts of $z \sim 2$–3).

Guerço et al. (2019) provided a glimpse into the overall behavior of F abundances across the Milky Way via the analysis of a sample of red giants spanning both a range of Galactocentric distances (R_g), as well metallicities, and found different trends of [F/Fe] versus [Fe/H] for the geometric thin and thick-disk red giants, as well as a hint that values of [F/Fe] might be elevated in the outer Galaxy. These results highlight the need to probe ^{19}F abundances in different stellar populations and locations in the Milky Way, such as the Galactic center.

The center of the Milky Way is host to a supermassive black hole, along with a nuclear stellar cluster (NSC), which is a common configuration in most massive galaxies (e.g., Schödel et al. 2014). The NSC is massive ($M_{NSC} \sim 2.5 \times 10^7 M_\odot$) and is composed of multiple stellar populations, with older red giant stars (having ages from 3–8 Gyr), along with young (10^7–10^8 yr) luminous massive stars (e.g., Nogueras-Lara et al. 2021). The primary goal of this study is to probe the fluorine abundances in a sample of red giants in the Galactic center (at distances from the center of ~2.5–30 pc) whose chemical abundances (not including ^{19}F) have been the subject of previous studies (Carr et al. 2000; Ramírez et al. 2000; Cunha et al. 2007; Davies et al. 2009; Najarro et al. 2009; Rich et al. 2017; Do et al. 2018; Thorsbro et al. 2020; see also Bentley et al. 2022) these stars sample a new and unique region of the Galaxy in which to map fluorine abundances.
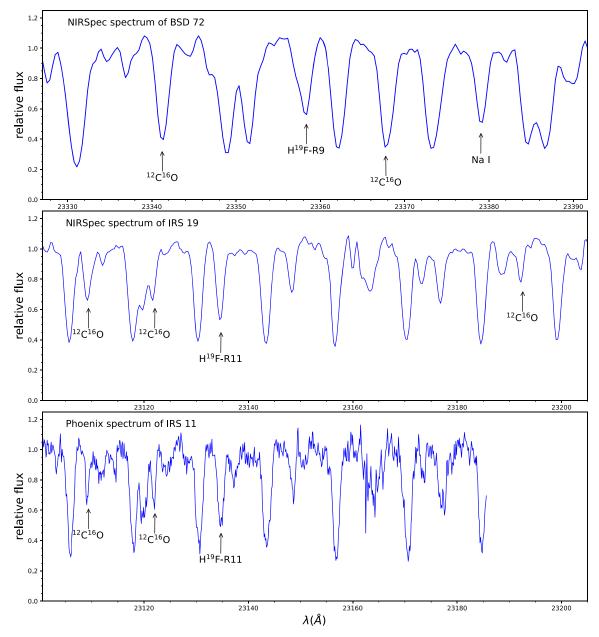
Figure 1. Sample spectra in the 2.3 μm region used in the abundance analysis. NIRSpec on board the Keck II telescope spectra are shown in the top and middle panels and a Phoenix spectrum on board the Gemini South telescope spectrum is shown in the bottom panel. The spectral region in the first panel includes the HF(1-0)R9 line, the Na I doublet (λ 23378.945 and 23379.139 Å) and two strong lines of CO (λ 23341.22 and 23379.139 Å); the spectral region in the middle and bottom panels includes the HF(1-0)R11 line and three weak lines of CO (λ 23109.370, 23122.097, and 23192.581 Å).

2. Observations

The targets are members of star clusters residing in the center of Milky Way previously studied in Cunha et al. (2007) and have been the subject of other previous studies (Carr et al. 2000; Ramírez et al. 2000; Davies et al. 2009). Five of the stars belong to the Nuclear cluster and one star is from the Quintuplet cluster. Table 1 summarizes the observations, gives the Two Micron All Sky Survey (2MASS) IDs when available, and their J, H, and K magnitudes.

The spectra analyzed here were obtained with the instruments NIRSpec ($R = \lambda/\Delta\lambda = 25{,}000$) on board the 10 m Keck II telescope and Phoenix ($R = \lambda/\Delta\lambda = 50{,}000$) on board the 8 m Gemini South telescope. The echelle order #33 NIRSpec spectra, with a lambda range from $\lambda23{,}100$–$\lambda23{,}420$ Å were analyzed; the

wavelength range for the Phoenix spectra are range from $\lambda23{,}095$–$\lambda23{,}200$ Å. The spectra were reduced in a standard way and followed the same basic steps and procedures as described, for example, in Cunha et al. (2007). In Figure 1 we show sample spectra of the Galactic sample targets and label the HF transitions along with CO lines analyzed (Table 2). The top and middle panels show NIRSpec spectra, including the HF-R9 and HF-R11 transitions, respectively. The bottom panel of Figure 1 shows a sample Phoenix spectrum in the H^{19}F-R11 region.

3. Abundance Analysis

The adopted values of effective temperature and surface gravity are presented in Table 1 and a corresponding Kiel diagram is presented in Figure 2; the Galactic center targets are
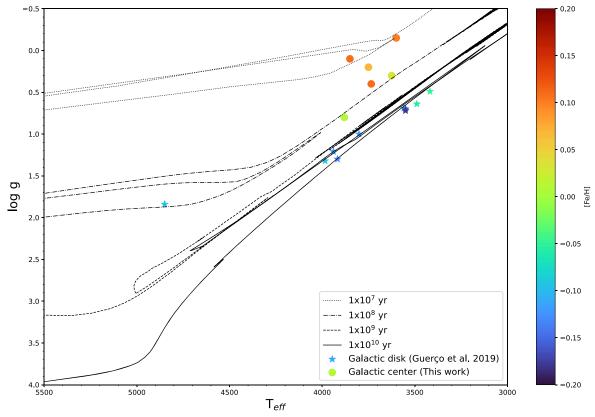
Figure 2. T_{eff}-log g diagram (Kiel diagram) for the luminous red giants in this sample are shown as filled circles; asterisks represent a subsample of stars from Guerço et al. (2019) having metallicities around solar; isochrones (from Bressan et al. 2012) for solar metallicities and ages 1×10^7 yr (dotted line), 1×10^8 yr (dotted–dashed line), 1×10^9 yr (dashed line) and 1×10^{10} yr (solid line) are also shown to illustrate relative positions on the RGB. The stars are color coded by metallicity between -0.2 and 0.2 dex.

Table 2
Line List

Molecule	λ_{air} (Å)	χ (eV)	log gf	D_o (eV)
H^{19}F(1–0)R9	23358.329	0.227[a][b]	−3.962[a]	5.869[c]
H^{19}F(1–0)R11	23134.757	0.332[a]	−3.942[a]	5.869[c]
^{12}C^{16}O(2–0)R80	23109.370	1.51[d]	−4.907[d]	11.092
^{12}C^{16}O(2–0)R81	23122.097	1.55[d]	−4.900[d]	11.092
^{12}C^{16}O(2–0)R86	23192.581	1.74[d]	−4.879[d]	11.092
^{12}C^{16}O(3–1)R26	23341.225	0.431[d]	−5.065[d]	11.092
^{12}C^{16}O(3–1)R4	23367.752	0.005[d]	−6.338[d]	11.092

Notes.
[a] Jönsson et al. (2014a).
[b] Decin (2000).
[c] Sauval & Tatum (1984).
[d] Goorvitch (1994).

cool (T_{eff} ranging from 3600–3850 K), evolved, and quite luminous, having log g values less than ∼0.4, with the exception of one target star that is less luminous (with log $g = 0.8$). The stellar parameters adopted for the studied targets were taken from Cunha et al. (2007). The effective temperatures in that study were based on spectral indices of CO and H$_2$O absorption, with the final T_{eff} being an average of results derived originally by Blum et al. (2003) and those obtained from a relation they constructed of T_{eff} with spectral type, which was based on effective temperatures derived in Smith & Lambert (1990). Log g values were obtained using the absolute bolometric magnitudes from Blum et al. (2003).

Fluorine abundances (Table 3) were derived by calculating synthetic spectra in local thermal equilibrium with the code Turbospectrum (TS; Alvarez & Plez 1998; Plez 2012) using the MARCS models atmosphere (Gustafsson et al. 2008) that we interpolate using the online grid of OSMARCS models[7] corresponding to 5–15 $M_{\odot}$. To compute best fits to the observed spectra, the BACCHUS wrapper (Masseron et al. 2016) was used in manual mode, including a single Gaussian to represent both the instrumental broadening and the macro-turbulent velocity.

The derivations of the fluorine abundances were based on two vibrational rotational HF (1–0) R9 and R11 transitions at $\lambda 2.3$ μm. The HF lines used in the abundance analyses are presented in the Table 2, with their excitation potentials (χ; from Jönsson et al. 2014a and Decin 2000), log gf-values (from Jönsson et al. 2014a), and the dissociation energy ($D_o = 5.869$ eV; from Sauval & Tatum 1984). Five strong CO lines found in the same spectral region where the HF lines reside (Table 2) were used in order to estimate the microturbulent velocity parameter (see discussion below) adjustments were made to the carbon abundances as needed in order to obtain good fits to the CO lines.

Abundance analyses based upon static model atmospheres typically require an additional small-scale line-broadening mechanism, usually added in as an extra velocity-broadening term referred to as microturbulence. The value of the microturbulent velocity (ξ) in a particular star is set by the

---

[7] http://marcs.astro.uu.se/

Table 3
Stellar Parameters and Abundances

Star	T_{eff}[a]	$\log g$[a]	ξ	Mass[a]	R_g[a]	A(Fe)[a]	A(C)	$^{16}O/^{17}O$	A(F)$_{R9}$	A(F)$_{R11}$	$\langle A(F) \rangle$
BSD 72	3880	0.80	4.15 ± 0.38	5.0	1.60	7.51	8.27 ± 0.14	95 ± 30	4.90	4.91	4.91 ± 0.01
BSD 124	3735	0.40	4.84 ± 0.27	6.5	1.90	7.61	8.18 ± 0.13	160 ± 40	4.80	4.85	4.83 ± 0.03
IRS 11	3625	0.30	2.30	4.5	0.62	7.53	8.40	$\cdots$	$\cdots$	4.38	4.38
IRS 19	3850	0.10	3.96 ± 0.24	15.	1.00	7.63	8.16 ± 0.21	390 ± 60	4.85	4.95	4.90 ± 0.05
IRS 22	3750	0.20	4.33	10.	1.00	7.57	8.09 ± 0.05	170 ± 30	4.74	4.75	4.75 ± 0.01
VR 5-7	3600	-0.15	4.57 ± 0.07	14.	31.0	7.60	7.82 ± 0.02	270 ± 30	4.75	4.75	4.75 ± 0.00

Note.
[a] Cunha et al. (2007).

Table 4
Abundance Sensitivities to Stellar Parameters

Element	$\delta T_{eff} = +100$ K	$\delta \log g = +0.25$	$\delta[Fe/H] = +0.10$	$\delta\xi = +0.25$ km · s^{-1}	ΔA[a]
F	$+0.20$	$+0.02$	$+0.05$	-0.02	± 0.21
C (weak CO lines)	$+0.06$	$+0.13$	$+0.13$	$+0.00$	± 0.19
C (strong CO lines)	$+0.06$	$+0.13$	$+0.13$	-0.04	± 0.20

Note. Baseline model: $T_{eff} = 3700$ K; $\log g = 0.50$; [Fe/H] = 0.00; $\xi = 4.50$ km s^{-1}.
[a] Total uncertainty in abundance is defined as $\Delta A = [(\delta T)^2 + (\delta \log g)^2 + (\delta [Fe/H])^2 + (\delta \xi)^2]^{1/2}$.

requirement that the derived abundance from a set of spectral lines of a specific species yield abundances that are independent of the line strength (more properly, the reduced equivalent width, W_λ/λ). Although usually assumed to be modeled by a single value, it has been found in previous analyses of cool luminous red giants that low-excitation, strong molecular lines, such as from CO or OH, require larger values of the microturbulent velocity when compared to higher excitation (and typically weaker) atomic or molecular lines (e.g., Smith & Lambert 1986, 1990; Tsuji 1988, 1991, 2008). As the HF lines analyzed in the Galactic center stars are low excitation and strong, values for ξ were set using a set of $^{12}C^{16}O$ lines that have a range of line strengths that overlap those of the H^{19}F lines. The microturbulent velocities are included in Table 1 and range from $\xi = 2.3$–4.8 km · s^{-1}, similar to values derived by Carr et al. (2000) for the Galactic center luminous cool supergiant IRS7 ($\xi = 3.0$ km · s^{-1}), and the supergiants α Ori ($\xi = 3.1$–3.8 km · s^{-1}), and VV Cep ($\xi = 3.5$–4.4 km · s^{-1}).

In addition to the numerous and strong $^{12}C^{16}O$ lines falling within the spectral region of the HF lines, there are also lines from $^{12}C^{17}O(2$–$0)$ running through the spectra around the HF-R9 line, with this line itself blended with the $^{12}C^{17}O(2$–$0)$ R25 line. Dredge-up on the RGB will bring an increased abundance of ^{17}O to the surface (along with ^{13}C), with ratios of $^{16}O/^{17}O$ decreasing from solar-like ratios of ~ 2750, to values as low as ~ 400–100 for masses greater than $2M_\odot$ (for recent studies of $^{16}O/^{17}O$ in various types of red giants, see Lebzelter et al. 2019a, 2019b). Since this sample of luminous red giants consists of rather massive stars ($M > 5M_\odot$), dredge-up on the RGB will result in detectable $^{12}C^{17}O$ lines near the H^{19}F R9 line. In order to improve the fit to the H^{19}F R9 line, it was necessary to determine the abundance of ^{17}O via the CO lines and these abundances, as ratios of $^{16}O/^{17}O$, are presented in Table 3. These ratios were derived from combinations of the $^{12}C^{17}O(2$–$0)$R25, R26, R27, R28, or R29 lines.

3.1. Abundance Uncertainties

Uncertainties in the derived F and C abundances were estimated establishing the sensitivity of these abundances to changes in the stellar parameters corresponding to their typical errors in T_{eff} (± 100 K), $\log g$ (± 0.25 dex), metallicity (± 0.10 dex), and microturbulent velocity (± 0.25 km · s^{-1}). The estimated uncertainties for each parameter and the square root of the sum in quadrature of the corresponding abundance ($\Delta A = [(\delta T)^2 + (\delta \log g)^2 + (\delta [Fe/H])^2 + (\delta \xi)^2]^{1/2}$) are presented in the Table 4. We used a baseline model atmosphere with $T_{eff} = 3700$ K, $\log g = 0.50$, [Fe/H] = 0.00, and $\xi = 4.50$ km s^{-1} to calculate the sensitivities of abundances with the disturbance δT, $\delta \log g$, δ [Fe/H] and $\delta \xi$.

4. Discussion

Figure 2 shows the Kiel diagram with the stellar parameters adopted in this study for the sample of Galactic center stars (filled circles). We also show for comparison those stars with metallicities > -0.2 dex from the disk sample analyzed previously in Guerço et al. (2019), as these will be used to define the disk trend around solar metallicities in the discussion of fluorine results. It is apparent from a comparison with the solar metallicity isochrones shown (Bressan et al. 2012) that the Galactic center targets are much younger and, thus, more massive, having ages between 10^7 and 10^8 yr, and masses in the range of $M \sim 6$–$16M_\odot$ (Cunha et al. 2007), when compared to the stars from the Galactic disk previously studied, which span ages from 10^9–10^{10} yr and masses of $M \sim 1$–$2M_\odot$. The more metal-poor disk targets in Guerço et al. (2019) are also older than the Galactic center population, as can be seen from Figure 2 in that paper.

4.1. Fluorine in the Galactic Center and the Disk

The [F/H] abundances obtained here for the sample of stars residing in the Galactic center, in conjunction with previous
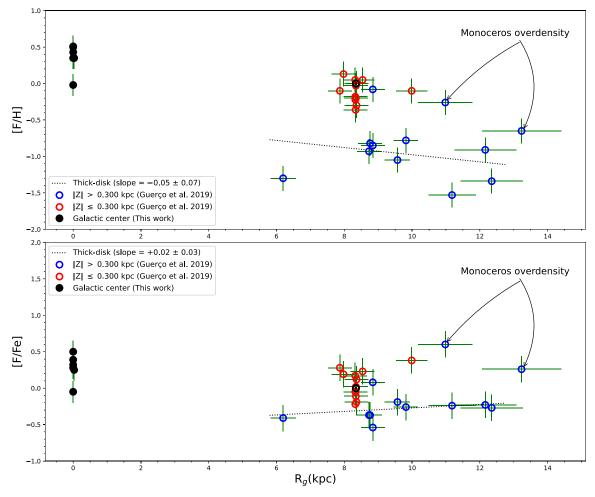
Figure 3. Top panel: [F/H] abundances as a function of the projected galactocentric distance, R_g; bottom panel: [F/Fe] abundances as a function of R_g. Black circles represent the Galactic center stars analyzed. The open circles are disk stars from Guerço et al. (2019). The dotted line represents the best-fit slope to disk stars with distances to the midplane >300 pc (blue circles taken as thick-disk stars, except the Monoceros overdensity stars). The distances of the Galactic center stars are from Cunha et al. (2007). The distances and uncertainties of the disk stars are based on Gaia EDR3 (Gaia Collaboration et al. 2021) and were taken from Bailer-Jones et al. (2021). The solar references for fluorine and iron are from Maiorca et al. (2014) and Asplund et al. (2009).

results obtained for disk stars, provide the opportunity to begin to explore possible radial variations in fluorine abundances in the Galactic disk. Within this context, it is important to note that rotating and non-rotating massive star models predict that fluorine abundances in stars having masses within the studied range are not expected to be destroyed (Ekström et al. 2012) and therefore their fluorine content would represent their natal cloud value. Figure 3 shows the [F/H] (top panel) and [F/Fe] (bottom panel) abundances versus galactocentric distances for fluorine results obtained homogeneously here (filled black circles) and in Guerço et al. (2019); the red open circles represent stars that are probable thin-disk members and the blue open circles probably belong to the thick disk, noting that the distinction between thick and thin in Guerço et al. (2019) comes solely from the distance, Z, a star has from the Galactic midplane. Given the uncertainties in the fluorine abundance determinations (see the sensitivity of the HF abundances to stellar parameters in Table 4), the fluorine content around the solar neighborhood (for stars within ±1 kpc from the Sun) is roughly solar: $\langle[F/H]\rangle = -0.09 \pm 0.15$ and $\langle[F/Fe]\rangle = 0.09 \pm 0.25$. (We use the solar fluorine of $A(F) = 4.40 \pm 0.25$ from Maiorca et al. 2014 in this comparison.) The results for

Galactic center population are slightly enhanced $\langle[F/H]\rangle = 0.35 \pm 0.18$ and $\langle[F/Fe]\rangle = 0.28 \pm 0.17$.

Guerço et al. (2019) trace a fluorine gradient for their probable thick-disk stars that have galactocentric distances between roughly 6 and 12 kpc; the best-fit slope to their data is also shown in Figure 3. At this point, however, it is not possible to reliably trace a fluorine gradient for the thin disk, first because the fluorine results at hand do not extend toward the inner Galaxy and second, because abundance gradients are expected to and have been shown to evolve with time (e.g., Minchev et al. 2013; Donor et al. 2020; Spina et al. 2021); thus, we would be mixing fluorine results for a young population with those of field disk stars of unknown ages. Simply combining the fluorine abundances for the thin disk, however, would result in a nearly null variation with galactocentric distance for the [F/Fe] ratio and a small negative slope for [F/H]. However, as discussed in Cunha et al. (2007) for iron, for example, the extrapolation of the metallicity gradient for the inner galaxy would predict a much higher metallicity for the Galactic center, which is not observed; the metallicity of the Galactic center young population is roughly solar or slightly above (Ramírez et al. 2000; Davies et al. 2009, etc.).
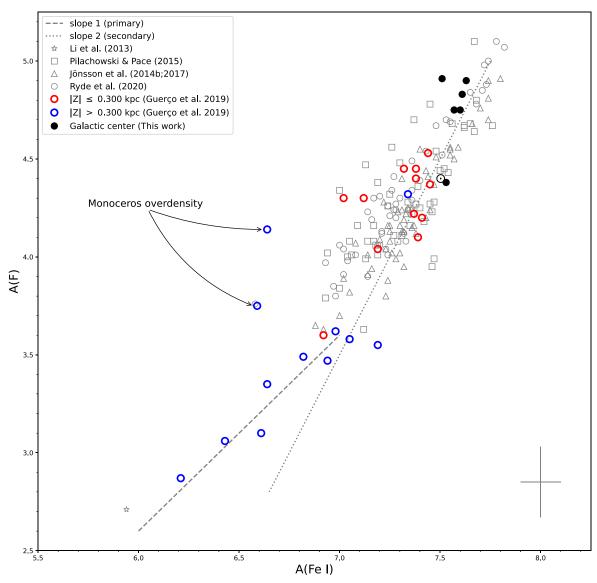
Figure 4. Behavior of the fluorine abundance with metallicity for the studied stars and previous results from the literature. Dashed lines representing pure primary and secondary behaviors for the change of fluorine with metallicity are also shown. The stars of Guerço et al. (2019) are segregated according to their distances, Z, from the Galactic midplane; the open blue circles correspond to probable thick-disk/halo stars, and the open red circles to probable thin-disk stars. Two stars identified as possible members of the Monoceros overdensity in Guerço et al. (2019) are marked. The black circles correspond to the results obtained in this work for the Galactic center stars. A representative error bar for the abundances is shown. The solar references for fluorine and iron are from Maiorca et al. (2014) and Asplund et al. (2009).

4.2. Chemical Evolution of Fluorine

Fluorine abundances as a function of metallicity from main studies in the literature are summarized in Figure 4. Again the black filled circles represent the Galactic center results from this study, while the open circles are the disk sample from Guerço et al. (2019), discussed above. We use the same symbols as before: in red are shown those stars having distances from the midplane $Z < 300$ pc and in blue those with $Z > 300$ pc.

Other results from the literature are also shown in Figure 4 as gray open symbols (Li et al. 2013; Jönsson et al. 2014b, 2017; Pilachowski & Pace 2015; Ryde et al. 2020). The overlap between the derived metallicities for A(Fe) > 7.0 ([Fe/H] > −0.5), where most of the results from the literature are found, is clear. A key aspect of the F versus Fe abundances in Figure 4, as noted and emphasized by Guerço et al. (2019), is the distinctive behaviors of A(F) as a function

of A(Fe) at lower metallicities when compared to higher metallicities (with A(Fe) ∼ 6.9–7.0 being the *transition* metallicity). The two lines in Figure 4 illustrate slopes of 1 (dashed) and 2 (dotted), which delineate primary and secondary yields, respectively, of ^{19}F when compared to Fe; the fluorine observed in the lower-metallicity stars arises from a primary-like source, while fluorine in the higher metallicity stars is dominated by a secondary-like source. In particular, the Galactic center fluorine abundances fall roughly within the distribution of results for those stars with metallicities above solar in the samples of Pilachowski & Pace (2015), (Jönsson et al. 2014b, 2017), or Ryde et al. (2020). Since the Galactic center stars sampled here are quite young, span a small range in metallicity, and may represent a distinct population, it is not possible to conclude that the same secondary-like source (or sources) that drives the chemical evolution in the thin disk is at work, but simply note
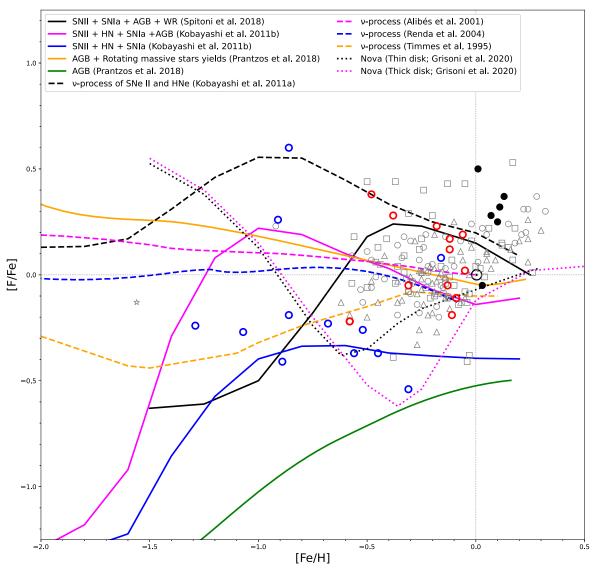
Figure 5. Chemical evolution of fluorine viewed as [F/Fe] versus [Fe/H]. The black circles correspond to the Galactic center stars from this work; the open blue circles correspond to probable thick-disk/halo stars and the open red circles to probable thin-disk stars from Guerço et al. (2019); all computed in the same scale as in this study. Results from other studies in the literature are shown as gray symbols (same as for Figure 4). Several chemical evolution models from the literature are also shown. The solar references for fluorine and iron are from Maiorca et al. (2014) and Asplund et al. (2009).

that the Galactic center fluorine abundances fall within the distribution of secondary-like behavior in disk stars.

There are uncertainties in both the derived F and Fe abundances and the impact of these uncertainties should be included as part of this discussion. As noted above, the young Galactic center stars, based upon the analysis here, are slightly more metal-rich than solar, with $\langle$[Fe/H]$\langle \sim +0.08$ and $\langle$[F/H]$\rangle \sim +0.35$. Since the F abundances are much more sensitive to $T_{\rm eff}$ than the Fe abundances, a small offset of -50 K in $T_{\rm eff}$ would result in values of both [Fe/H] and [F/H] $\sim +0.1$, with [F/Fe] ~ 0.0. Our results, when viewed in light of likely uncertainties in combinations of $T_{\rm eff}$ and log g, indicate that the young Galactic center stars have near-solar Fe and F abundances to slightly metal-rich stars with modest enhancements of F, with the stars falling along the secondary-like trend of fluorine relative to Fe.

Figure 5 illustrates a variety of Galactic chemical evolution models that include various sources for the nucleosynthesis of ^{19}F, plotting [F/Fe] versus [Fe/H], and including the

abundances derived here for the Galactic center stars shown as filled black circles. Also included are the abundances from Guerço et al. (2019) and the other observational studies, as discussed in the previous paragraph, the various observational studies are in good agreement. Guerço et al. (2019) discussed most of the chemical evolution models shown in Figure 5 in some detail, and here we review briefly these models and where the Galactic center abundances fit in. With [F/Fe] plotted as a function of [Fe/H] in Figure 5, primary chemical evolution would be flat (slope~0), while secondary would have a slope of 1. In general, this is the behavior seen in the derived abundance ratios from the sample in Guerço et al. (2019). Alas, as discussed previously, the Galactic center young stars, given their small range in metallicity, do not shed new light on the primary-like and secondary-like ^{19}F sources other than the fact that their [F/Fe] values are not in contrast with those of disk stars at the same iron abundances.

The rather large number of chemical evolution models displayed in Figure 5 may look bewildering at first glance, but

do illustrate the significant uncertainties regarding the origin(s) of fluorine and the corresponding stellar yields, and careful inspection can simplify the behaviors of the various models (see also the discussion in Grisoni et al. 2020). In general, most of the models in Figure 5 tend to converge to having roughly solar [F/Fe] (with boundaries at roughly [F/Fe] = +0.2 and −0.1) at [Fe/H] ∼ 0.0. This is not unexpected as the solar reference is commonly used to constrain models of the solar neighborhood, and in fact, the fluorine-over-iron abundances for solar neighborhood stars also scatter around solar (as also shown in Figure 4). In addition to the models shown in Figure 5, Olive & Vangioni (2019) scale neutrino process contributions using constraints from observed B11/B10 ratios, and find that AGB stars are the main contributors at solar metallicity, obtaining a flat and roughly solar behavior for [F/Fe] between [Fe/H] ∼ −1 and solar.

Focusing solely on the predicted model values of [F/Fe] for metallicities above solar, we note that all the above 1-zone models were constructed mainly for the solar neighborhood; stars with super-solar metallicities now found in the solar neighborhood, are thought to have originated from the inner disk, which has super-solar metallicity gas, via radial migration and in a timescale of a few gigayears. The models shown therefore may not be as meaningful in such high-metallicity regimes. The models by Kobayashi et al. (2011a) and Spitoni et al. (2018) are the only ones that predict enhanced values of [F/Fe] at metallicities slightly above solar, as seen for the Galactic center stars, but such models find a decrease in [F/Fe] as the metallicity increases. All of the other models shown in Figure 5 do not reach values of [F/Fe] above solar for [Fe/H] > 0. The fluorine results shown in Figure 5 corroborate this point: stars in the different fluorine studies (Jönsson et al. 2017; Ryde et al. 2020; Pilachowski & Pace 2015) having metallicities of solar and above (0.0 < [Fe/H] < +0.3) also show increased values of [F/Fe], an increase in [F/Fe] with metallicity for Fe/H > 0 as seen in the fluorine data for disk stars and the Galactic center is not predicted by any of the models.

Focusing on the predictions of [F/Fe] at the lowest metallicities shown in Figure 5 ([Fe/H] < −1.7) does show that all of the models predict primary-like evolution in [F/Fe]. In fact, the solid black (Spitoni et al. 2018), magenta, and blue (Kobayashi et al. 2011b) lines show secondary behavior; Timmes et al. (1995), Alibés et al. (2001), Renda et al. (2004), and Kobayashi et al. (2011b) (see also Olive & Vangioni 2019) find the ν-process to be a source of primary ^{19}F at these low metallicities.

Prantzos et al. (2018) adopt yields from rapidly rotating massive stars from Limongi & Chieffi (2018), where rotationally induced mixing results in the synthesis of primary ^{14}N and subsequently primary ^{19}F in He burning. This is an important difference between the neutrino-induced nucleo-synthesis and rotationally induced mixing; the former produces primary F from neutrino spallation of Ne, but does not affect N, which is normally made as secondary from C+O; in contrast, the latter produces both N and F as primaries, and this is a distinctive signature of rotation induced nucleosynthesis.

Given these models, with suitable adjustments to their yields and/or prescriptions for chemical evolution model details, a primary-like behavior of [F/Fe] in the lower-metallicity thick-disk population would result from either the ν-process or rapidly rotating massive stars, or a combination of the two. But

the observed primary-like behavior of N in the low-metallicity Galaxy (halo and thick disk) convincingly suggests that rotation is at play at low metallicities and provides an economic way to explain both N and F, if the latter really behaves as primary. The ν-mechanism is more uncertain, basically because of the uncertainty in the neutrino spectra of CCSN. The two stars at low metallicity with rather high values of [F/Fe] are ignored in this discussion, as they have been reported to be possible members of the Monoceros overdensity, which has been identified as a metal-poor stellar overdensity found ∼1–3 kpc out of the Galactic plane (Crane et al. 2003; Ibata et al. 2003; Rocha-Pinto et al. 2003; Morganson et al. 2016). If members of an independent stellar population, these two stars likely formed from gas which has undergone chemical evolution that is distinct from either of the thick or thin-disk populations.

On the other hand, high rotation cannot be invoked at slightly sub-solar and ∼solar metallicities, because s-elements are highly overproduced (see discussion in Prantzos et al. 2018). AGB stars, or perhaps, novae could be invoked for those metallicities. However, it should be noticed that detailed massive star yields for super-solar initial metallicities do not exist, with the exception of that found in Nomoto et al. (2013). As mentioned above, the secondary-like evolution of [F/Fe] in the more metal-rich thin-disk stars, including the mono-metallicity young stars in the Galactic center studied here, is not accounted for by any of the models, although the increasing values of [F/Fe] in the late thin disk and the Galactic center require some other sources, TP-AGB stars, novae, and/or W-R stellar winds.

One speculative source that is not included in the models noted here would be the H-deficient extreme He stars found by Pandey (2006), Werner & Herwig (2006), Pandey et al. (2008), and Bhowmick et al. (2020) to be enormously overabundant in fluorine, which probably result from double-degenerate mergers between a CO white dwarf and a He white dwarf (Menon et al. 2013; Lauer et al. 2019; Menon et al. 2019). Such systems may be too rare to have an impact on the Galactic ^{19}F budget, but might be worth investigating.

5. Conclusions

Fluorine abundances have been derived in six massive young luminous red giants in the Galactic center; five of the stars are members of the NSC, which is centered on the central supermassive black hole (SMBH), while the sixth is a member of the Quintuplet cluster (offset from the SMBH by ∼30 pc). The NSC is massive (∼2.5 × 10^7 $M_\odot$), containing several generations of stars with ages ranging from ∼10 Gyr to <10^7 yr (Nogueras-Lara et al. 2021), and a significant spread in metallicity (Thorsbro et al. 2020). The luminous red giants analyzed here are young and evolved, with ages ∼10^7–10^8 yr and masses of $M \sim 6$–$16\ M_\odot$. The ^{19}F abundances presented in this study are the first to be measured in the Galactic center, providing a view into the chemical evolution of fluorine in a unique region and population of the Milky Way. A by-product of the analysis of the spectral region near the HF(1 − 0) R9 line is the derivation of ^{16}O/^{17}O ratios; the RGB dredge-up of ^{17}O is a function of stellar mass making the ^{16}O/^{17}O ratios a sensitive probe of stellar nucleosynthesis and mixing along the RGB (e.g., Lebzelter et al. 2015). A more extensive study of the CNO isotopic abundances of the Galactic center red giants is in preparation.

The population of Galactic center luminous young red giants have been analyzed for their Fe abundances in previous studies (Ramírez et al. 2000; Cunha et al. 2007; Davies et al. 2009; Najarro et al. 2009), all of which have found near-solar to slightly elevated [Fe/H] abundances. In particular, Cunha et al. (2007) derived iron abundances for the cluster members studied here, and when combined with our F abundances, results in a mean value of $\langle[F/Fe]\rangle = +0.28 \pm 0.17$; these [F/Fe] ratios are roughly within the scatter of values for those stars previously studied near the Sun (with $R_{gal} \sim 8$–10 kpc). The small evolution in the [F/Fe] ratios between the solar neighborhood and the Galactic center suggest that any radial gradients in [F/Fe] are likely small in the inner Galaxy, although it should be kept in mind that field stars in the inner galactic region between the solar neighborhood and the center of the Milky Way have yet to be probed.

Concerning the behavior of fluorine versus metallicity, we find that the fluorine abundances in the Galactic center sample generally overlap with those of disk stars at similar metallicities, with the latter following a secondary-like trend compared to Fe (e.g., Guerço et al. 2019; Ryde et al. 2020); [F/Fe] ratios are found to be marginally elevated in this sample of Galactic center stars, pointing to increasing [F/Fe] ratios with increasing [Fe/H]. Since the Galactic center stars are quite young and do not span a range in metallicity, it is not possible to conclude that the same secondary-like source that drives the chemical evolution in the thin disk is at work. The observed increase of [F/Fe] with [Fe/H] is not predicted by any of the chemical evolution models discussed and presented in Figure 5, suggesting that quantifying the major source of ^{19}F at high metallicities remains elusive.

ORCID iDs

Rafael Guerço ● https://orcid.org/0000-0002-0151-5212
Katia Cunha ● https://orcid.org/0000-0001-6476-0576
Verne V. Smith ● https://orcid.org/0000-0002-0134-2024
Nikos Prantzos ● https://orcid.org/0000-0002-4591-6253
Kris Sellgren ● https://orcid.org/0000-0003-0817-2862
Simone Daflon ● https://orcid.org/0000-0001-9205-2307

References

Abia, C., Cristallo, S., Cunha, K., de Laverny, P., & Smith, V. V. 2019, A&A, 625, A40
Abia, C., Cunha, K., Cristallo, S., et al. 2010, ApJL, 715, L94
Abia, C., Cunha, K., Cristallo, S., & de Laverny, P. 2015, A&A, 581, A88
Abia, C., Recio-Blanco, A., de Laverny, P., et al. 2009, ApJ, 694, 971
Alibés, A., Labay, J., & Canal, R. 2001, A&A, 370, 1103
Alvarez, R., & Plez, B. 1998, A&A, 330, 1109
Asplund, M., Grevesse, N., Sauval, A. J., & Scott, P. 2009, ARA&A, 47, 481
Bailer-Jones, C. A. L., Rybizki, J., Fouesneau, M., Demleitner, M., & Andrae, R. 2021, AJ, 161, 147
Bentley, R. O., Do, T., Kerzendorf, W., et al. 2022, ApJ, 925, 77
Bhowmick, A., Pandey, G., & Lambert, D. L. 2020, ApJ, 891, 40
Blum, R. D., Ramirez, S. V., Sellgren, K., & Olsen, K. 2003, ApJ, 597, 323
Bressan, A., Marigo, P., Girardi, L., et al. 2012, MNRAS, 427, 127
Carr, J. S., Sellgren, K., & Balachandran, S. C. 2000, ApJ, 530, 307
Clayton, G. C., Geballe, T. R., Herwig, F., Fryer, C., & Asplund, M. 2007, ApJ, 662, 1220
Crane, J. D., Majewski, S. R., Rocha-Pinto, H. J., et al. 2003, ApJL, 594, L119
Cunha, K., Sellgren, K., Smith, V. V., et al. 2007, ApJ, 669, 1011
Cunha, K., Smith, V. V., & Gibson, B. K. 2008, ApJL, 679, L17
Cunha, K., Smith, V. V., Lambert, D. L., & Hinkle, K. H. 2003, AJ, 126, 1305
Davies, B., Origlia, L., Kudritzki, R.-P., et al. 2009, ApJ, 694, 46
Decin, L. 2000, PhD thesis, Catholique Univ. Leuven
Do, T., Kerzendorf, W., Konopacky, Q., et al. 2018, ApJL, 855, L5
Donor, J., Frinchaboy, P. M., Cunha, K., et al. 2020, AJ, 159, 199
Ekström, S., Georgy, C., Eggenberger, P., et al. 2012, A&A, 537, A146
Federman, S. R., Sheffer, Y., Lambert, D. L., & Smith, V. V. 2005, ApJ, 619, 884
Franco, M., Coppin, K. E. K., Geach, J. E., et al. 2021, NatAs, 5, 1240
Gaia Collaboration, Brown, A. G. A., Vallenari, A., et al. 2021, A&A, 649, A1
Goorvitch, D. 1994, ApJS, 95, 535
Grisoni, V., Romano, D., Spitoni, E., et al. 2020, MNRAS, 498, 1252
Guerço, R., Cunha, K., Smith, V. V., et al. 2019, ApJ, 885, 139
Gustafsson, B., Edvardsson, B., Eriksson, K., et al. 2008, A&A, 486, 951
Ibata, R. A., Irwin, M. J., Lewis, G. F., et al. 2003, MNRAS, 340, L21
Jönsson, H., Ryde, N., Harper, G. M., et al. 2014a, A&A, 564, A122
Jönsson, H., Ryde, N., Harper, G. M., Richter, M. J., & Hinkle, K. H. 2014b, ApJL, 789, L41
Jönsson, H., Ryde, N., Spitoni, E., et al. 2017, ApJ, 835, 50
Jorissen, A., Smith, V. V., & Lambert, D. L. 1992, A&A, 261, 164
Kobayashi, C., Izutani, N., Karakas, A. I., et al. 2011a, ApJL, 739, L57
Kobayashi, C., Karakas, A. I., & Umeda, H. 2011b, MNRAS, 414, 3231
Lauer, A., Chatzopoulos, E., Clayton, G. C., Frank, J., & Marcello, D. C. 2019, MNRAS, 488, 438
Lebzelter, T., Hinkle, K., & Straniero, O. 2019a, IAUS, 343, 447
Lebzelter, T., Hinkle, K. H., Straniero, O., Lambert, D. L., Pilachowski, C. A., & Nault, K. A. 2019b, ApJ, 886, 117
Lebzelter, T., Straniero, O., Hinkle, K. H., Nowotny, W., & Aringer, B. 2015, A&A, 578, A33
Li, H. N., Ludwig, H.-G., Caffau, E., Christlieb, N., & Zhao, G. 2013, ApJ, 765, 51
Limongi, M., & Chieffi, A. 2018, ApJS, 237, 13
Maiorca, E., Uitenbroek, H., Uttenthaler, S., et al. 2014, ApJ, 788, 149
Masseron, T., Merle, T., & Hawkins, K. 2016, BACCHUS: Brussels Automatic Code for Characterizing High accUracy Spectra, Astrophysics Source Code Library, ascl:1605.004
Menon, A., Herwig, F., Denissenkov, P. A., et al. 2013, ApJ, 772, 59
Menon, A., Karakas, A. I., Lugaro, M., Doherty, C. L., & Ritter, C. 2019, MNRAS, 482, 2320
Meynet, G., & Arnould, M. 2000, A&A, 355, 176
Minchev, I., Chiappini, C., & Martig, M. 2013, A&A, 558, A9
Morganson, E., Conn, B., Rix, H.-W., et al. 2016, ApJ, 825, 140
Najarro, F., Figer, D. F., Hillier, D. J., Geballe, T. R., & Kudritzki, R. P. 2009, ApJ, 691, 1816
Nogueras-Lara, F., Schödel, R., & Neumayer, N. 2021, ApJ, 920, 97
Nomoto, K., Kobayashi, C., & Tominaga, N. 2013, ARA&A, 51, 457
Olive, K. A., & Vangioni, E. 2019, MNRAS, 490, 4307
Palacios, A., Arnould, M., & Meynet, G. 2005, A&A, 443, 243
Pandey, G. 2006, ApJL, 648, L143
Pandey, G., Lambert, D. L., & Kameswara Rao, N. 2008, ApJ, 674, 1068
Pilachowski, C. A., & Pace, C. 2015, AJ, 150, 66
Plez, B. 2012, Turbospectrum: Code for Spectral Synthesis, Astrophysics Source Code Library, ascl:1205.004
Prantzos, N., Abia, C., Limongi, M., Chieffi, A., & Cristallo, S. 2018, MNRAS, 476, 3432
Ramírez, S. V., Sellgren, K., Carr, J. S., et al. 2000, ApJ, 537, 205
Renda, A., Fenner, Y., Gibson, B. K., et al. 2004, MNRAS, 354, 575
Rich, R. M., Ryde, N., Thorsbro, B., et al. 2017, AJ, 154, 239
Rocha-Pinto, H. J., Majewski, S. R., Skrutskie, M. F., et al. 2003, ApJL, 594, L115
Ryde, N., Jönsson, H., Mace, G., et al. 2020, ApJ, 893, 37
Sauval, A. J., & Tatum, J. B. 1984, ApJS, 56, 193

Schödel, R., Feldmeier, A., Kunneriath, D., et al. 2014, A&A, 566, A47
Smith, V. V., Cunha, K., Ivans, I. I., et al. 2005, ApJ, 633, 392
Smith, V. V., & Lambert, D. L. 1986, ApJ, 311, 843
Smith, V. V., & Lambert, D. L. 1990, ApJS, 72, 387
Sneden, C., Bean, J., Ivans, I., Lucatello, S., & Sobeck, J. 2012, MOOG: LTE Line analysis and spectrum synthesis, Astrophysics Source Code Library, ascl:1202.009
Soubiran, C., Le Campion, J.-F., Brouillet, N., & Chemin, L. 2016, A&A, 591, A118
Spina, L., Ting, Y.-S., De Silva, G. M., et al. 2021, MNRAS, 503, 3279
Spitoni, E., Matteucci, F., Jönsson, H., Ryde, N., & Romano, D. 2018, A&A, 612, A16
Thorsbro, B., Ryde, N., Rich, R. M., et al. 2020, ApJ, 894, 26
Timmes, F. X., Woosley, S. E., & Weaver, T. A. 1995, ApJS, 98, 617
Tody, D. 1986, Proc. SPIE, 627, 733

Tody, D. 1993, in ASP Conf. Ser. 52, Astronomical Data Analysis Software and Systems II, ed. R. J Hanisch, R. J. V. Brissenden, & J. Barnes (San Francisco, CA: ASP), 173
Tsuji, T. 1988, A&A, 197, 185
Tsuji, T. 1991, A&A, 245, 203
Tsuji, T. 2008, A&A, 489, 1271
Uttenthaler, S., Aringer, B., Lebzelter, T., et al. 2008, ApJ, 682, 509
Werner, K., & Herwig, F. 2006, PASP, 118, 183
Werner, W., Rauch, T., & Kruk, J. W. 2006, in ASP Conf. Ser. 348, Insight into AGB and post-AGB Stellar Evolution with FUSE (San Francisco, CA: ASP), 191
Woosley, S. E., Hartmann, D. H., Hoffman, R. D., & Haxton, W. C. 1990, ApJ, 356, 272
Woosley, S. E., & Haxton, W. C. 1988, Natur, 334, 45
Yong, D., Meléndez, J., Cunha, K., et al. 2008, ApJ, 689, 1020